Accepted Manuscript

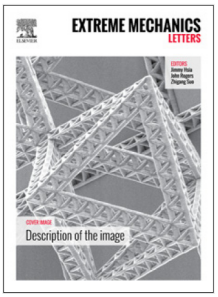

The elastic fields of a compressible liquid inclusion

Xin Chen, Moxiao Li, Mao Yang, Shaobao Liu, Guy M. Genin, Feng Xu, Tian Jian Lu

PII: S2352-4316(18)30033-6
DOI: https://doi.org/10.1016/j.eml.2018.06.002
Reference: EML 379

To appear in: *Extreme Mechanics Letters*

Received date : 4 March 2018
Revised date : 23 May 2018
Accepted date : 4 June 2018

Please cite this article as: X. Chen, M. Li, M. Yang, S. Liu, G.M. Genin, F. Xu, T.J. Lu, The elastic fields of a compressible liquid inclusion, *Extreme Mechanics Letters* (2018), https://doi.org/10.1016/j.eml.2018.06.002

The elastic fields of a compressible liquid inclusion

Xin Chen [a,b,c], Moxiao Li [a,b,c], Mao Yang [a,b,c], Shaobao Liu [c,d], Guy M. Genin [c,d,e], Feng Xu [c,d#], Tian Jian Lu [a,b,c#]

[a] *State Key Laboratory for Strength and Vibration of Mechanical Structures, Xi'an Jiaotong University, Xi'an 710049, P.R. China*

[b] *MOE Key Laboratory for Multifunctional Materials and Structures, Xi'an Jiaotong University, Xi'an 710049, PR China*

[c] *Bioinspired Engineering and Biomechanics Center (BEBC), Xi'an Jiaotong University, Xi'an 710049, P.R. China*

[d] *The Key Laboratory of Biomedical Information Engineering of Ministry of Education, Xi'an Jiaotong University, Xi'an 710049, P.R. China*

[e] *U.S. National Science Foundation Science and Technology Center for Engineering Mechanobiology, Washington University, St. Louis, MO 63130 USA*

[#] *Corresponding authors: fengxu@mail.xjtu.edu.cn, tjlu@mail.xjtu.edu.cn*

Abstract: Elastic composites containing liquid inclusions exist widely in rocks, food, tissues and hydrogels. We investigate a single ellipsoidal compressible liquid inclusion embedded in an infinite elastic matrix, such as an isolated cell embedded in an extracellular matrix and oil or gas pocket embedded within shale. We first derive the displacement and stress fields in the matrix under far field loading. For the special case of a spherical inclusion, we arrive at simple, explicit expressions for these fields. We next focus on the shape evolution of the liquid inclusion and the stress concentration in the matrix, from which we conclude when the effect of liquid compressibility is most significant. Finally, we classify common examples of liquid inclusions in nature and engineering. According to our theoretical results, we estimate the importance of liquid compressibility in these examples and provide guidelines for further application of the theory of liquid inclusions in practical situations.

Keywords: liquid inclusion, liquid compressibility, inclusion theory, solid-liquid interaction

1. Introduction

Elastic composites [1] with liquid inclusions exist widely in nature and engineering, including rocks, food, tissues and hydrogels. Accumulating evidence has shown that the elastic fields of such composites (e.g., the deformation and stress state in and outside the inclusions) are important for their widespread applications in biology [2], geology [3], materials science [4, 5] and bionic engineering [6]. For instance, the deformation and stress state of cells in a three-dimensional (3D) matrix under far field loading could significantly affect their differentiation [7]. Elastic composites with liquid inclusions have been well studied from the mechanical perspective, where the inclusions are often simplified to two limiting cases, i.e., infinite compressibility (e.g., cracks in rocks [8]) and incompressibility (e.g., droplets in soft materials [9]). However, significant differences in elastic fields between cavities (i.e., infinite compressibility) and incompressible fluid inclusions have been observed, indicating the importance of fluid compressibility. Therefore, it is necessary to derive elastic fields both inside and outside a compressible liquid inclusion in an elastic matrix under far field loadings, such as a cell embedded in extracellular matrix or oil/gas deposit trapped within shale.

The framework for addressing this problem is the seminal work of Eshelby, who solved for the response of a single ellipsoidal elastic solid inclusion in an infinite elastic matrix subjected to far field loadings [10]. As will be described below, we follow Eshelby's framework and make minor adaptations to enable its application to compressible, ellipsoidal, liquid inclusions. Although this problem has been approached using experimental [11-13] and simulation approaches [14], no complete solution has been published for the detailed elastic fields both within and outside the inclusion. This paper addresses that need, and furthermore explores the nature of these elastic fields, and how they may be used to tailor the mechanics of a composite material or tissue.

We note that parts of this solution have been published before. The complete solutions

have been published for the two limiting cases: an ellipsoidal void in an infinite elastic matrix (infinite compressibility), and an incompressible, ellipsoidal fluid pocket within an infinite elastic matrix. The solution for the ellipsoidal void follows directly from Eshelby's solution, and is well known [15]. The solution for an incompressible, ellipsoidal fluid droplet under uniaxial loading was derived by Style *et al.* [9] using stress potential functions. The elastic fields within a compressible, ellipsoidal fluid pocket and the shape change of that ellipsoid were derived by Shafiro *et al.* [16] and David *et al.* [17] using Eshelby's approach. These solutions, as one would predict from the Eshelby solution, have uniform stress and strain fields. However, explicit expressions for the elastic fields in the matrix have not been published. Therefore, this paper presents the full solution for the elastic fields within and outside a compressible, ellipsoidal fluid inclusion; identifies cases both for which this solution is important and for which the previously published limiting cases are adequate; and explores a range of surprising behaviors that are revealed by this solution.

In this paper, we consider an isolated ellipsoidal compressible liquid inclusion embedded within an infinite elastic matrix. We first derive the displacement and stress fields in the matrix under far field loading. We next focus on the shape evolution of the liquid inclusion and the stress concentration in the matrix. From these mechanical responses of the inclusion and matrix, we conclude when the effect of liquid compressibility is most significant. Finally, we classify the common examples of liquid inclusions in nature and engineering. According to our theoretical results, we estimate the importance of liquid compressibility in practical applications by grouping these examples into three broad categories (*i.e.*, geological, biological and engineering two-phase composites). Our results provide useful guidelines for further application of the theory of liquid inclusions in practice.

2. Statement of the problem

We begin by considering an isolated ellipsoidal liquid inclusion imbedded within an

infinite and linear elastic matrix (**Figure 1a**). We assume the initial pressure of the liquid is zero so that the matrix is free of stress before far field loading. We further assume that the liquid inclusion is sufficiently large that surface effects at the liquid-matrix interface may be neglected. Upon loading, according to the theory of linear elasticity, the governing equations in the matrix are

$$\begin{aligned} &\boldsymbol{\varepsilon} = \frac{1}{2}\left(\nabla \mathbf{u} + \mathbf{u}\nabla\right), \\ &\boldsymbol{\sigma} = \frac{E}{1+\nu}\left[\frac{\nu}{1-2\nu}\mathrm{tr}\left(\boldsymbol{\varepsilon}\right) + \boldsymbol{\varepsilon}\right], \\ &\nabla \cdot \boldsymbol{\sigma} = 0. \end{aligned} \tag{1}$$

where $\mathbf{u}$, $\boldsymbol{\varepsilon}$ and $\boldsymbol{\sigma}$ are the displacement vector, linearized strain tensor, and engineering stress tensor in the matrix, respectively, and E (N/m^2) and ν are Young's modulus and Poisson ratio of the matrix material.

Let the liquid be linearly compressible, namely [16]

$$k\frac{\Delta V}{V} = -p, \tag{2}$$

where k (N/m^2) is the bulk modulus of the liquid, V and ΔV are the initial volume and change in volume of the inclusion, respectively, and p is the liquid pressure after loading.

We assume the strain tensor within the matrix at far field in Cartesian coordinates (**Figure 1**) is given by

$$\boldsymbol{\varepsilon}\big|_{|x|\to\infty} = \boldsymbol{\varepsilon}^{\infty} \tag{3}$$

where $\boldsymbol{\varepsilon}^{\infty}$ is a constant strain tensor.

At the interface between the inclusion and matrix, the stress of the matrix is balanced by the liquid pressure, as

$$\boldsymbol{\sigma} \cdot \mathbf{n} = -p\mathbf{n} \tag{4}$$

where $\mathbf{n}$ is the unit outward vector of the interface.

3. Solution of the problem

We solve the problem by the equivalent inclusion method of Eshelby [10]. The solution for the ellipsoidal inclusion is given by elliptic functions in section 3.1. To investigate the effect of liquid compressibility, we derive the explicit expressions for the problem of a spherical liquid inclusion in 3.2.

3.1 Elastic fields for ellipsoidal inclusion

In this part, we will solve the problem of the ellipsoidal liquid inclusion by the equivalent method from Eshelby [10]. We will follow the language of Eshelby (i.e. eigenstrain and eigenstress) in this part.

We first note that the stress fields in the liquid inclusion are uniform (*i.e.* hydrostatic stress) under far field loading. We consider an imaginary problem: an infinite linear elastic matrix I contains an ellipsoidal domain Ω which sustains a uniform eigenstrain $\boldsymbol{\varepsilon}^*$. We assume that the ellipsoidal domain Ω has the same shape as the liquid inclusion in our original problem stated in Section 2, and the matrix has the same far field load eq. (3). According to Eshelby, the stress fields in the domain Ω are also uniform. The equivalent method is that if we choose a proper $\boldsymbol{\varepsilon}^*$ such that the liquid inclusion in the original problem has the same deformation and stress fields as the domain Ω in the imaginary problem, then the two problems will have the same elastic fields in their matrix.

For the imaginary problem, the strain in the domain Ω is $\boldsymbol{\varepsilon}^{\infty} + \mathbf{S} : \boldsymbol{\varepsilon}^*$ by the principle of superposition, where $\mathbf{S}$ is the Eshelby tensor for the ellipsoidal domain. The stress in the domain is

$$\boldsymbol{\sigma}^{img} = \mathbf{L}_0 : \left(\mathbf{S} : \boldsymbol{\varepsilon}^* - \boldsymbol{\varepsilon}^* + \boldsymbol{\varepsilon}^{\infty} \right) \tag{5}$$

where the fourth-rank tensor $\mathbf{L}_0$ is the stiffness tensor of the matrix, with components:

$$\left(\mathbf{L}_0\right)_{ijkl} = \frac{E\nu}{\left(1+\nu\right)\left(1-2\nu\right)}\delta_{ij}\delta_{kl} + \frac{E}{1+\nu}\delta_{ik}\delta_{jl}$$

in which δ_{ij} is Kroncker's delta function. For the original problem of liquid inclusion, if the deformation of the liquid inclusion is the same as that of the domain Ω in the imaginary problem, *i.e.* $\boldsymbol{\varepsilon}^{\infty} + \mathbf{S} : \boldsymbol{\varepsilon}^{*}$, the stress in the liquid inclusion is

$$\boldsymbol{\sigma}^{liquid} = \mathbf{L}_1 : \left(\mathbf{S} : \boldsymbol{\varepsilon}^{*} + \boldsymbol{\varepsilon}^{\infty}\right) \tag{6}$$

where the fourth-rank tensor $\mathbf{L}_1$ is the "stiffness tensor" of the liquid, *i.e.*,

$$\left(\mathbf{L}_1\right)_{ijkl} = k\delta_{ij}\delta_{kl}.$$

If we equate the stress in the liquid inclusion with the that of the domain Ω in the imaginary problem, *i.e.*,

$$\boldsymbol{\sigma}^{img} = \boldsymbol{\sigma}^{liquid}, \tag{7}$$

we can determine the eigenstrain $\boldsymbol{\varepsilon}^{*}$ from equations (5), (6) and (7) as

$$\boldsymbol{\varepsilon}^{*} = -\left[\left(\mathbf{L}_1 - \mathbf{L}_0\right)^{-1} : \mathbf{L}_0 + \mathbf{S}\right] : \boldsymbol{\varepsilon}^{\infty}. \tag{8}$$

Then the volume variation and pressure of the liquid inclusion (same as the domain Ω) can be expressed by the imaginary problem as

$$\frac{\Delta V}{V} = \mathrm{tr}\left(\boldsymbol{\varepsilon}^{\infty} + \mathbf{S} : \boldsymbol{\varepsilon}^{*}\right) = \mathrm{tr}\left\{\left[\mathbf{I} + \mathbf{S} : \mathbf{L}_0^{-1} : \left(\mathbf{L}_1 - \mathbf{L}_0\right)\right]^{-1} : \boldsymbol{\varepsilon}^{\infty}\right\}, \tag{9}$$

and

$$p = k \cdot \mathrm{tr}\left\{\left[\mathbf{I} + \mathbf{S} : \mathbf{L}_0^{-1} : \left(\mathbf{L}_1 - \mathbf{L}_0\right)\right]^{-1} : \boldsymbol{\varepsilon}^{\infty}\right\}, \tag{10}$$

respectively, where $\mathrm{tr}\left(\cdot\right)$ is the trace of the second-order tensor.

The displacement fields in the matrix for the two problems are

$$\mathbf{u}\left(\mathbf{x}\right) = \mathbf{B}\left(\mathbf{x}\right) : \boldsymbol{\varepsilon}^{*} + \boldsymbol{\varepsilon}^{\infty} \cdot \mathbf{x}, \tag{11}$$

where $\mathbf{B}\left(\mathbf{x}\right)$ are third-rank tensors, which can be expressed by some elliptic integrals. Details can be seen in [15, 18].

To investigate the physical meaning of the solution, we decompose the matrix

deformation into two parts, *i.e.*, the deformation of a void cavity induced by far field load (**Figure 1b**), and the deformation induced by inner pressure p (**Figure 1c**). Based on this decomposition, we divide the eigenstrain into two parts:

$$\boldsymbol{\varepsilon}^{*} = \boldsymbol{\varepsilon}_{c}^{*} + \boldsymbol{\varepsilon}_{p}^{*}, \tag{12}$$

where

$$\begin{aligned} \boldsymbol{\varepsilon}_{c}^{*} &= -\left[-\mathbf{I}+\mathbf{S}\right]:\boldsymbol{\varepsilon}^{\infty}, \\ \boldsymbol{\varepsilon}_{p}^{*} &= \left\{\left[-\mathbf{I}+\mathbf{S}\right]-\left[\left(\mathbf{L}_{1}-\mathbf{L}_{0}\right)^{-1}:\mathbf{L}_{0}+\mathbf{S}\right]\right\}:\boldsymbol{\varepsilon}^{\infty}. \end{aligned} \tag{13}$$

Then the displacement fields in the matrix can be rewritten as

$$\mathbf{u}\left(\mathbf{x}\right) = \left[\boldsymbol{\varepsilon}^{\infty}\cdot\mathbf{x} + \mathbf{B}\left(\mathbf{x}\right):\boldsymbol{\varepsilon}_{c}^{*}\right] + \mathbf{B}\left(\mathbf{x}\right):\boldsymbol{\varepsilon}_{p}^{*}, \tag{14}$$

where the first part is the matrix deformation of the void cavity induced by far field load and the second part is the matrix deformation induced by inner pressure.

Because the components of $\mathbf{S}$ are zero except for S_{iijj} and S_{ijij} $(i,j=1,2,3)$, we observe from equation (13) that $\boldsymbol{\varepsilon}_{p}^{*}=\mathbf{0}$ when the far field load $\boldsymbol{\varepsilon}^{\infty}$ is simple shear. In other words, the liquid inclusion behaves like a void cavity (no pressure variation) under simple shear. This coincides with Biot's treatment of liquids for porous material [19]: liquid contributes only to the resistance to normal stress, and not to the resistance to shear stress. Because of this, we consider only the far field uni-axial load to investigate the effect of liquid compressibility in the following. Then the matrix strain at far field in Cartesian coordinates (**Figure 1**) is given by

$$\boldsymbol{\varepsilon}^{\infty} = \begin{pmatrix} \varepsilon & 0 & 0 \\ 0 & -\nu\varepsilon & 0 \\ 0 & 0 & -\nu\varepsilon \end{pmatrix}, \tag{15}$$

where $\varepsilon>0$ represents stretching and $\varepsilon<0$ represents compression.

3.2 Explicit expressions for spherical liquid inclusion

For a spherical liquid inclusion, the expressions of (9), (10) and (11) can be written explicitly. Due to symmetry, we write these expressions in spherical polar coordinates

(**Figure 1a**). The volume variation (9) and pressure (10) of the liquid inclusion reduce to

$$\begin{aligned} \frac{\Delta V}{V} &= \frac{3(1-\nu)}{2+3\bar{k}(1+\nu)}\varepsilon, \\ p &= -\frac{3\bar{k}(1-\nu)}{2+3\bar{k}(1+\nu)}E\varepsilon, \end{aligned} \tag{16}$$

where $\bar{k}$ is the ratio of the liquid bulk modulus to the solid Young's modulus:

$$\bar{k} = \frac{k}{E}.$$

To avoid singularity when the matrix is incompressible, we normalize the liquid bulk modulus k by the solid Young's modulus E rather than by the solid bulk modulus. The displacement fields (11) in the matrix can be written as

$$\begin{aligned} u_r &= B_1 r + B_2 \frac{R^3}{r^2} \\ &\quad + \frac{3\cos 2\theta + 1}{4}\left[12\nu A_1 \frac{r^3}{R^2} + 2A_2 r + 2(5-4\nu)A_3 \frac{R^3}{r^2} - 3A_4 \frac{R^5}{r^4}\right] \\ u_\theta &= -\frac{3\sin 2\theta}{2}\left[(7-4\nu)A_1 \frac{r^3}{R^2} + A_2 r + 2(1-2\nu)A_3 \frac{R^3}{r^2} + A_4 \frac{R^5}{r^4}\right] \end{aligned} \tag{17}$$

where A_i ($i = 1, 2, 3, 4$) and B_j ($j = 1, 2$) are

$$\begin{aligned} A_1 &= 0, \\ A_2 &= \frac{1-2\nu}{3}\varepsilon, \\ B_1 &= \frac{1+\nu}{3}\varepsilon, \\ A_3 &= \frac{5(1+\nu)}{6(7-5\nu)}\varepsilon, \\ A_4 &= \frac{1+\nu}{7-5\nu}\varepsilon, \\ B_2 &= \frac{(1+\nu)\left[1-3\bar{k}(1-2\nu)\right]}{6+9\bar{k}(1+\nu)}\varepsilon, \end{aligned} \tag{18}$$

We observe that the liquid compressibility $\bar{k}$ only appears only in the coefficient B_2 for the displacement fields (18). In other words, liquid compressibility only

affects the radial deformation.

Substituting (17) into (1), we arrive at the stress fields in the matrix

$$\begin{aligned}
\sigma_{rr} &= \frac{E}{1+\nu}\left\{ B_1 \frac{1+\nu}{1-2\nu} - 2B_2 \frac{R^3}{r^3} \right. \\
&\quad \left. + \frac{3\cos 2\theta + 1}{4}\left[-6\nu A_1 \frac{r^2}{R^2} + 2A_2 - 4(5-4\nu) A_3 \frac{R^3}{r^3} + 12 A_4 \frac{R^5}{r^5} \right] \right\}, \\
\sigma_{r\theta} &= -\frac{3\sin 2\theta}{2} \frac{E}{1+\nu}\left[(7+2\nu) A_1 \frac{r^2}{R^2} + A_2 + 2(1+\nu) A_3 \frac{R^3}{r^3} - 4A_4 \frac{R^5}{r^5} \right], \\
\sigma_{\theta\theta} &= \frac{E}{4(1+\nu)}\left\{ \left[\frac{4(1+\nu)}{1-2\nu} B_1 + \frac{4(1-\nu)}{1-2\nu} \frac{R^2}{r^2} B_2 \right] \right. \\
&\quad -6\left[5\nu + 7(2+\nu)\cos 2\theta \right] A_1 \frac{r^2}{R^2} - 2(-1+3\cos 2\theta) A_2 \\
&\quad \left. +2(1-2\nu)(5+3\cos 2\theta) A_3 \frac{R^3}{r^3} - (3+7\cos 2\theta) A_4 \frac{R^5}{r^5} \right\}.
\end{aligned} \tag{19}$$

Similar to the decomposition in Section 3.1, we rewrite the displacement fields by substituting (16) and (18) into (17), as

$$\begin{aligned}
u_r &= \frac{1-2\nu}{3}\varepsilon r + \frac{1}{6}(1+\nu)\frac{R^3}{r^2}\varepsilon + \frac{1}{2}\frac{p}{E}(1+\nu)\frac{R^3}{r^2} \\
&\quad + \frac{3\cos 2\theta + 1}{4}\left[2\frac{1+\nu}{3} r + \frac{5(1+\nu)(5-4\nu)}{3(7-5\nu)} \frac{R^3}{r^2} - 3\frac{1+\nu}{7-5\nu}\frac{R^5}{r^4} \right]\varepsilon, \\
u_\theta &= -\frac{3\sin 2\theta}{2}\left[\frac{1+\nu}{3} r + \frac{5(1+\nu)(1-2\nu)}{3(7-5\nu)} \frac{R^3}{r^2} + \frac{(1+\nu)}{7-5\nu}\frac{R^5}{r^4} \right]\varepsilon.
\end{aligned} \tag{20}$$

From (20), we can see that the deformation in the matrix can be decomposed into two parts (**Figure 1b** and **c**), *i.e.*, the deformation of a void cavity, and the radial deformation induced by liquid pressure. In other words, this reveals once more that the effect of liquid compressibility on matrix deformation is to enhance radial deformation.

4. Results and discussion

We will investigate the effect of liquid compressibility in this section. We focus on the deformation of ellipsoidal inclusions in 4.1, the shape and pressure of spherical inclusions in 4.2, and the stress concentration outside of spherical inclusions in 4.3.

4.1 Effective strain of ellipsoidal inclusion

To verify our solution, we first compare it with two limiting cases, i.e., the incompressible limit and the void cavity limit. Following Style et al. [9], to characterize the sensitivity of the axial deformation of the inclusion to far field load, we consider the "effective strain" ε_{eff} (**Figure 2a**) as defined by

$$\varepsilon_{eff} = \frac{u}{a} = \left[\boldsymbol{\varepsilon}^{\infty} + \mathbf{S} : \boldsymbol{\varepsilon}^{*}\right]_{11}, \tag{22}$$

where a is the half length of the inclusion in the load direction, u is the displacement magnitude of the tips of the inclusion in the load direction, and $\left[\boldsymbol{\varepsilon}^{\infty} + \mathbf{S} : \boldsymbol{\varepsilon}^{*}\right]_{11}$ means the $(1,1)$ component of the tensor $\boldsymbol{\varepsilon}^{\infty} + \mathbf{S} : \boldsymbol{\varepsilon}^{*}$.

To assess the transition between the two well-known limits, we plot the dimensionless effective strain $\frac{\varepsilon_{eff}}{\varepsilon}$ as a function of liquid compressibility $\frac{k}{E}$ in **Figure 2b**. This quantity is central to dipole treatments of composite materials [20, 21], and is referred to as a "strain factor" in biophysical theories of tissues [22, 23]. We consider different shapes of ellipsoidal inclusions (aspect ratios of $1:1:1$, $1.5:1:1$ and $2:1:1$), and uniaxial far field loading along the direction of longest axis. For the case of low bulk modulus, the effective strain decreases with $\frac{k}{E}$ for all aspect ratios, dropping from an asymptote for the case of a void to that for the case of an incompressible fluid; these asymptotes match those reported in the literature ([9], [15, 24]). Consistent with study of strain factors for solid inclusions, the effective strain of the spherical inclusion is greater than those for general ellipsoidal inclusions [25, 26]. Considering the qualitative similarity of trends observed for spheres and ellipsoids, we focus on the spherical inclusion to investigate the effect of liquid compressibility in the following for convenience.

4.2 Deformation and pressure of the spherical liquid inclusion

The relationship between volume and pressure is an important mechanical property of the liquid inclusion. For instance, the pressure influences the effective Young's modulus of composites with liquid inclusions [27, 28]. **Figure 3a** and **Figure 3b** show how liquid compressibility affects the volume variation and pressure of liquid inclusions as induced by far field loading. We observe that if the liquid is nearly incompressible, the change of inclusion volume is negligible but the pressure (absolute value) is maximized. As the liquid compressibility increases, the change of liquid volume $\Delta V/V$ increases and the pressure p (absolute value) decreases. The compressibility effect is greatest when the bulk modulus of the liquid and the Young's modulus of the solid are on the same order of magnitude. When approaching the two limiting cases (a cavity and an incompressible liquid), the compressibility of the inclusion has no significant influence on either the volume change or the pressure of the liquid inclusion.

The solutions we present in **Figure 3a**, integrated with advanced imaging, enable estimation of the bulk modulus if the mechanical properties of the matrix are known [29]. Such measurements have been made for isolated cells [30] and chondrocyte cells in compressed articular cartilage [31] using confocal microscopy. A range of systems exist for making these measurements for tissues and engineered microenvironments that load cells in tension [32]. Note that cells typically undergo a transition from solid-like to fluid-like at strains sufficient to depolymerize their actin cytoskeletons [33], and are in general compressible in both cases [31]. From the perspective of engineering materials, in a material system of water inclusions in polydimethylsiloxane, the size and volume of inclusions can be determined by ultra-deep microscopy [11].

Following loading, we observe from (17) that liquid inclusions becomes ellipsoidal. The aspect ratio of the ellipsoidal inclusion can be derived from equation (17):

$$\lambda_I = \frac{(7-5\nu)\left[2+3\bar{k}(1+\nu)\right]+3\left[2\nu(1+5\nu)+\bar{k}\left(7-2\nu+11\nu^2+20\nu^3\right)\right]\varepsilon}{(7-5\nu)\left[2+3\bar{k}(1+\nu)\right]-3\left[8\nu+\bar{k}\left(-7+17\nu+19\nu^2-5\nu^3\right)\right]\varepsilon}. \quad (23)$$

Over the range of small strains, the effect of liquid compressibility on λ_I is only a few percent (**Figure 3c**, plotted for $\varepsilon = 0.1$). However, the effect of the Poisson ratio of the matrix is far greater.

To explain this weak dependence of aspect ratio on the compressibility of the inclusion, we use the decomposition described above. That is, we decomposed the deformation of the liquid inclusion into the deformation of a void cavity superimposed upon the radial deformation induced by liquid pressure. According to equation (16), we can estimate the liquid pressure after the uniaxial load is applied as:

$$\left|\frac{p}{E\varepsilon}\right| = \left|\frac{3\bar{k}(1-\nu)}{2+3\bar{k}(1+\nu)}\right| \le 1, \quad \bar{k} \in [0,\infty), \nu \in [0,0.5], \quad (24)$$

which can be proved by direct calculations. Then we can estimate the radial displacement of the inclusion boundary induced by liquid pressure, as:

$$\left|\frac{1}{2}\frac{p}{E}(1+\nu)\frac{R^3}{r^2}\right|_{r=R} \le \frac{1+\nu}{2}R\left|\frac{p}{E\varepsilon}\right|\varepsilon \le 0.75\varepsilon R. \quad (25)$$

In this estimation, we use the inequalities $0 \le \nu \le 0.5$ and $\left|\frac{p}{E\varepsilon}\right| \le 1$. For $\varepsilon = 0.1$, the radial displacement of the inclusion boundary is less than $0.075R$, and the length of the long and short axis of the deformed inclusion is $1.40R$ and $0.90R$, respectively. The radial displacement of the inclusion boundary induced by liquid pressure is too small to influence the inclusion aspect ratio.

4.2 Stress concentration near the liquid inclusion

The macroscopic strength of a two-phase composite is strongly dependent on stress concentration by inclusions. According to the Tresca yield criterion, the solid will yield when the maximum shear stress exceeds a critical value. According to the

explicit expression of stress fields (18), we calculate the maximum shear stress $\tau_{\max}$ in the matrix (details are presented in the **Supplementary material**). We show the normalized maximum shear stress $\tau_{\max}/\tau_{\max}^{\infty}$ near the inclusion as a function of liquid compressibility in **Figure 4**, where $\tau_{\max}^{\infty}=\dfrac{E\varepsilon}{2}$ is the far field maximum shear stress. We observe that, on one hand, if the solid is compressible (i.e., $\nu<0.5$), there is a transition point at which the maximum shear stress is minimum. In other words, there is an optimal liquid compressibility for minimal stress concentration outside the inclusion. This transition occurs when the liquid bulk modulus and the Young's modulus of solid are on the same order of magnitude. On the other hand, if the solid is incompressible (i.e., $\nu=0.5$), the maximum shear stress monolithically decreases as the liquid incompressibility increases. This suggests that tailoring the compressibility of liquid inclusions can increase the macroscopic strength of a composite.

To understand the transition phenomenon, with the Poisson ratio of the matrix fixed at $\nu=0.3$, we plot in **Figure 4** the maximum shear stress near the inclusion for selected values of liquid compressibility. When the liquid compressibility is increased, we find that the location of the maximum shear stress transfers from the tip of the inclusion in the load direction (point A in **Figure 1**) to the tip in the free direction (point B in **Figure 1**). At the transition point, the maximum shear stress at A is equal to that at B. We can formulate the maximum shear stresses at A and B as

$$\begin{aligned}\tau_A&=\frac{3\left[1+5\nu+3\bar{k}\left(4-3\nu+5\nu^2\right)\right]}{2\left(7-5\nu\right)\left[2+3\bar{k}\left(1+\nu\right)\right]}E\varepsilon,\\ \tau_B&=\frac{3\left[9-5\nu+3\bar{k}\left(1+8\nu-5\nu^2\right)\right]}{2\left(7-5\nu\right)\left[2+3\bar{k}\left(1+\nu\right)\right]}E\varepsilon.\end{aligned}\tag{26}$$

By solving $\tau_A=\tau_B$, we find the transition point is dependent only on the Poisson ratio of the matrix:

$$\bar{k}_{transition}=\frac{2\left(4-5\nu\right)}{3(3-11\nu+10\nu^2)}.\tag{27}$$

This is the transition line plotted in **Figure 4**. Correspondingly, we can also calculate the critical value of the maximum shear stress at the transition point, as:

$$\tau_{critical} = \frac{15E\varepsilon}{2(14-10\nu)}. \tag{28}$$

In order to further investigate the impact of liquid compressibility on stress concentration, we plot the normalized maximum shear stress as a function of the liquid bulk modulus as well as the elastic modulus and Poisson ratio of the solid in **Figure 5**. Within the region of sensitivity between the two dashed lines, the maximum shear stress is sensitive to the normalized liquid bulk modulus k/E. The minimum of $\tau_{\max}/\tau_{\max}^{\infty}$ occurs when the liquid bulk modulus and the solid elastic modulus have the same magnitude ($k/E \sim 1$). This important property of liquid inclusions can be favorably exploited for materials design targeting both engineering and biological applications. For example, we can reduce the stress concentration around inclusions for porous materials by choosing proper liquid fillers. Furthermore, this provides insight into the benefit of compressibility that has been observed in cells such as articular chondrocytes [31]. These results may have implications for the mechanisms underlying cell migration in a soft matrix.

According to the results above, we find that the effect of liquid compressibility is greatest when the bulk modulus of the liquid and the Young's modulus of the solid are on the same order of magnitude. This provides a criterion to judge whether considering the compressibility of liquid in practical applications. If $\frac{k}{E} < 0.1$ (e.g., liquid-gas mixture in rocks [8]), the inclusion has the same properties as cavity. If $\frac{k}{E} > 10$ (e.g., liquid droplet in hydrogel [11]), the liquid in the inclusion can be treated as incompressible liquid. If $0.1 \le \frac{k}{E} \le 10$ (e.g., cells in bones [34-36]), we must consider liquid compressibility.

5. Compressibility in composites with liquid inclusions

To further apply the analytical results, we collect common examples in nature and engineering. Although this paper deals with liquid inclusions, in the mechanical analysis we only make two fundamental assumptions about the liquid: (1) it is compressible; (2) it can transmit only normal force to the matrix. Consequently, the results obtained can also be used for inclusions of a gas or a gas-liquid mixture.

The case of a gas-liquid inclusion is particularly interesting. For a pure substance, the gas-liquid mixture is saturated. When the far field load is applied, the pressure of the inclusion remains constant and the volume fraction of liquid in the inclusion changes. Therefore, the inclusion volume will change. At this time, the inclusion behaves like a void cavity. The matrix deformation is described by eq. (14) by setting the inclusion bulk modulus $k = 0$.

If the gas-liquid mixture is a mixture (such as a gas-liquid mixture in rocks), in general, the gas and liquid are not saturated. Under the assumption of small deformation of the matrix, we can ignore the phase transition and estimate the bulk modulus $k_{mixture}$ by liquid bulk modulus k_{liquid} and gas bulk modulus k_{gas} through a harmonic average [37] (details can be seen in **Supplementary material**):

$$k_{mixture} = \frac{1}{\dfrac{\phi_{gas}}{k_{gas}} + \dfrac{\phi_{liquid}}{k_{liquid}}} \tag{29}$$

where ϕ_{gas} and ϕ_{liquid} are volume fraction of gas and liquid, respectively.

If $k_{liquid} \quad k_{gas}$, the bulk modulus of the mixture can be estimated as

$$k_{mixture} = \frac{k_{gas}}{\phi_{gas}} \tag{30}$$

At this time, the matrix deformation is described by eq. (14) by setting the inclusion bulk modulus as (29) or (30).

For application, we present selected examples of two-phase elastic composites in the $(\bar{k},\nu)$ space in an Ashby-type plot (**Figure 6**). These examples are classified into three categories, i.e., geological materials, biological materials and engineering materials (**Supplementary material**). Geological materials are mainly rocks containing gas, oil or water. In these materials, the liquid bulk modulus k often has a smaller magnitude than with the solid elastic modulus E, and the solid often has a relatively low Poisson ratio ($\nu < 0.4$). Thus, geological materials are distributed in the lower left corner of the $(\bar{k},\nu)$ space. According to our theoretical results, liquid compressibility must be considered for liquid-gas mixture inclusions and is negligible for liquid inclusions. This is consistent with the earlier findings that approximate liquid-gas mixture inclusions by cavity [8].

Biological examples include a very broad range of normalized moduli, ranging from a compliant cell such as a chondrocyte embedded in a relatively stiff tissue, to a stiff, activated fibroblast invading a compliant granulation tissue in wound healing. The mechanical properties (Young's modulus E and Poisson ratio ν) of human tissue changes greatly, so that the selected examples are widely distributed in this space. In both **Figure 6** and the **Supplementary material**, the cells are taken as nearly incompressible. However, due to mass transfer across cell membrane, cells can change their volume under load, which makes the compressibility of cells complex [31, 38-40]. Consequently, for biological examples, the inclusion compressibility must be considered. According to the results of **Figure 4 and Figure 5**, to minimize stress concentration, cells prefer to be surrounded by tissues having similar properties. Similar phenomena have been observed in experiments, with cells changing their mechanical properties to match the stiffness of their extracellular matrix [23, 41-43].

Engineering materials are mainly elastic composites with distributed liquid or gas inclusions. Because the matrix materials are often polymers (e.g., rubber or gel) with high Poisson ratios, these materials are distributed toward the top of the space

($\nu > 0.4$). According to our theoretical results, the compressibility must be considered for both gas inclusions and gas-fluid mixture inclusions while the limit of incompressible inclusion [9] can be used for liquid inclusions.

6. Conclusion

In this paper, a unified mechanical model is established to analyze the elastic field of compressible liquid inclusions which are common in nature and engineering. An explicit analytical solution to the problem is given. Deformation and pressure evolution of the liquid inclusion is analyzed. It is found that when the bulk modulus k of the liquid inclusion and the elastic modulus E of the solid matrix are on the same order of magnitude, liquid compressibility has the greatest effect on the volume and pressure of the inclusion.

Stress concentration around the liquid inclusion is attenuated by optimal compressibility of the liquid inclusions. There is an optimal value of liquid compressibility for which the peak shear stress in the matrix is lower than either the stress concentration around a void in that matrix, or the stress concentration around an incompressible liquid inclusion. The present results have interesting implications for design of composite materials: tailoring the compressibility of liquid inclusions can increase the macroscopic strength of a composite. The results furthermore provide a putative explanation for why cells remodel themselves and their local environments to match the mechanical properties of their microenvironment.

Finally, common examples of liquid inclusions in nature and engineering are classified. We analyze the role of liquid compressibility in each category. For the mechanical analysis of liquid inclusions, in practice, our results show that for all three classes of materials, there exist ranges over which compressibility must be considered (**Figure 6.**) For cases with very high or very low effective compressibility, the material can be separately modeled using the void cavity model [8, 15] or

incompressible liquid inclusion model [9]. For the case of $k/E \sim 1$, the significant influence of compressibility on the mechanical system needs to be specially considered.

We conclude with some caveats about two key assumptions in the article. The first is that the study is applicable to cases where the inclusions are sufficiently large that surface energy is not a factor in the mechanics of the composite. When the size of the liquid inclusion gradually becomes smaller, the influence of the surface energy gradually becomes greater. According to previous literature, the surface energy affects the elastic field around liquid inclusions [9], and it couples with the compressibility of inclusions. This can in certain cases lead to elastic instability [44-46]. The role of surface energy will be considered in the sequel. A second limitation is that only isolated liquid pockets were considered. Interactions between inclusions increase up to a percolation threshold, beyond which the effective strain (strain factor) approaches unity and the rule of mixtures begins to apply to the composite [25, 26]. The effects of liquid inclusions on this approach to percolation, and the effects of elastic interactions on such effects [47], represent important future directions of inquiry.

Acknowledgements

This work was supported by the National Natural Science Foundation of China (11372243, 11522219, 11532009), by the National Institutes of Health through grant U01EB016422, and by the National Science Foundation through the Science and Technology Center for Engineering Mechanobiology, grant CMMI 1548571.

References

[1] O. Vincent, P. Marmottant, P.A. Quinto-Su, C.-D. Ohl, Birth and growth of cavitation bubbles within water under tension confined in a simple synthetic tree, Phys. Rev. Lett., 108 (18) (2012) 184502.

[2] O. Campàs, T. Mammoto, S. Hasso, R.A. Sperling, D. O'Connell, A.G. Bischof, R. Maas, D.A. Weitz, L. Mahadevan, D.E. Ingber, Quantifying cell-generated mechanical forces within living

embryonic tissues, Nat. Methods, 11 (2) (2014) 183.
[3] T. Poulet, M. Veveakis, A viscoplastic approach for pore collapse in saturated soft rocks using REDBACK: An open-source parallel simulator for Rock mEchanics with Dissipative feedBACKs, Comput. Geotech., 74 (in press) (2016) 211-221.
[4] P.S. Owuor, S. Hiremath, A.C. Chipara, R. Vajtai, J. Lou, D.R. Mahapatra, C.S. Tiwary, P.M. Ajayan, Nature Inspired Strategy to Enhance Mechanical Properties via Liquid Reinforcement, Adv. Mater. Interfaces, 4 (16) (2017).
[5] F. Mancarella, R.W. Style, J.S. Wettlaufer, Interfacial tension and a three-phase generalized self-consistent theory of non-dilute soft composite solids, Soft Matter, 12 (10) (2016) 2744.
[6] A. Miriyev, K. Stack, H. Lipson, Soft material for soft actuators, Nat. Commun., 8 (1) (2017) 596.
[7] N. Huebsch, P.R. Arany, A.S. Mao, D. Shvartsman, O.A. Ali, S.A. Bencherif, J. Rivera-Feliciano, D.J. Mooney, Harnessing traction-mediated manipulation of the cell-matrix interface to control stem cell fate, Nat. Mater., 9 (6) (2010) 518.
[8] B. Budiansky, R.J. O'Connell, Elastic moduli of a cracked solid, Int. J. Solids Struct., 12 (2) (1976) 81-97.
[9] R.W. Style, J.S. Wettlaufer, E.R. Dufresne, Surface tension and the mechanics of liquid inclusions in compliant solids, Soft Matter, 11 (4) (2015) 672-679.
[10] J.D. Eshelby, The determination of the elastic field of an ellipsoidal inclusion, and related problems, P. Roy. Soc. A, 241 (1226) (1957) 376-396.
[11] R.W. Style, R. Boltyanskiy, B. Allen, K.E. Jensen, H.P. Foote, John S. Wettlaufer, E.R. Dufresne, Stiffening solids with liquid inclusions, Nat. Phys., 11 (1) (2014) 82-87.
[12] L. Ducloué, O. Pitois, J. Goyon, X. Chateau, G. Ovarlez, Coupling of elasticity to capillarity in soft aerated materials, Soft Matter, 10 (28) (2014) 5093.
[13] O. Vincent, P. Marmottant, P.A. Quinto-Su, C.D. Ohl, Birth and growth of cavitation bubbles within water under tension confined in a simple synthetic tree, Phys. Rev. Lett., 108 (108) (2011) 184502.
[14] Y. Wang, D.L. Henann, Finite-element modeling of soft solids with liquid inclusions, Extreme Mechanics Letters, 9 (2016) 147-157.
[15] T. Mura, Micromechanics of Defects in Solids, Springer Science & Business Media, 2013.
[16] B. Shafiro, M. Kachanov, Materials with fluid-filled pores of various shapes: Effective elastic properties and fluid pressure polarization, Int. J. Solids Struct., 34 (27) (1997) 3517-3540.
[17] E.C. David, R.W. Zimmerman, Compressibility and shear compliance of spheroidal pores: Exact derivation via the Eshelby tensor, and asymptotic expressions in limiting cases, Int. J. Solids Struct., 48 (5) (2011) 680-686.
[18] S. John, I. Leighton, C.I. Ye, Mechanical Analysis of Single Myocyte Contraction in a 3-D Elastic Matrix, PLoS One, 8 (10) (2013) e75492.
[19] M.A. Biot, General Theory of Three dimensional Consolidation, Journal of Applied Physics, 12 (1941).
[20] G.I. Zahalak, J.E. Wagenseil, T. Wakatsuki, E.L. Elson, A Cell-Based Constitutive Relation for Bio-Artificial Tissues, Biophys. J., 79 (5) (2000) 2369-2381.
[21] A. Zemel, F. Rehfeldt, A.E. Brown, D.E. Discher, S.A. Safran, Optimal matrix rigidity for stress fiber polarization in stem cells, Nat. Phys., 6 (6) (2010) 468-473.
[22] R. Kaunas, A. Zemel, Cell and matrix mechanics, CRC Press, Taylor & Francis Group, 2014.
[23] J.P. Marquez, G.M. Genin, Whole cell mechanics of contractile fibroblasts: relations between

effective cellular and extracellular matrix moduli, Philosophical Transactions, 368 (1912) (2010) 635.
[24] A.E.H. Love, A Treatise on the Mathematical Theory of Elasticity, Cambridge University Press, 2011.
[25] J.P. Marquez, G.M. Genin, G.I. Zahalak, E.L. Elson, The Relationship between Cell and Tissue Strain in Three-Dimensional Bio-Artificial Tissues, Biophys. J., 88 (2) (2005) 778-789.
[26] J.P. Marquez, G.M. Genin, G.I. Zahalak, E.L. Elson, Thin Bio-Artificial Tissues in Plane Stress: The Relationship between Cell and Tissue Strain, and an Improved Constitutive Model, Biophys. J., 88 (2) (2005) 765-777.
[27] M.L. Kachanov, B. Shafiro, I. Tsukrov, Handbook of Elasticity Solutions, Springer Science & Business Media, 2013.
[28] L. Dormieux, D. Kondo, F.-J. Ulm, Microporomechanics, John Wiley & Sons, 2006.
[29] C. Neu, Handbook of Imaging in Biological Mechanics, CRC Press, 2014.
[30] F. Guilak, Volume and surface area measurement of viable chondrocytes in situ using geometric modelling of serial confocal sections, Journal of Microscopy, 173 (3) (1994) 245-256.
[31] F. Guilak, A. Ratcliffe, V.C. Mow, Chondrocyte deformation and local tissue strain in articular cartilage: a confocal microscopy study, J. Orthop. Res., 13 (3) (1995) 410-421.
[32] W.R. Legant, J.S. Miller, B.L. Blakely, D.M. Cohen, G.M. Genin, C.S. Chen, Measurement of mechanical tractions exerted by cells in three-dimensional matrices, Nat. Methods, 7 (12) (2010) 969.
[33] C. Chen, R. Krishnan, E. Zhou, A. Ramachandran, D. Tambe, K. Rajendran, R.M. Adam, L. Deng, J.J. Fredberg, Fluidization and resolidification of the human bladder smooth muscle cell in response to transient stretch, PLoS One, 5 (8) (2010) e12035.
[34] D. Hartono, Y. Liu, P.L. Tan, X.Y. Then, L.Y. Yung, K.M. Lim, On-chip measurements of cell compressibility via acoustic radiation, Lab Chip, 11 (23) (2011) 4072.
[35] R.M. Pidaparti, A. Vogt, Experimental investigation of Poisson's ratio as a damage parameter for bone fatigue, J. Biomed. Mater. Res. A, 59 (2) (2002) 282-287.
[36] A.H. Burstein, D.T. Reilly, M. Martens, Aging of bone tissue: mechanical properties, J. Bone. Joint. Surg. Am., 58 (1) (1976) 82.
[37] S. Torquato, Random Heterogeneous Materials, Springer New York, 2002.
[38] K.M. Stroka, H. Jiang, S.H. Chen, Z. Tong, D. Wirtz, S.X. Sun, K. Konstantopoulos, Water permeation drives tumor cell migration in confined microenvironments, Cell, 157 (3) (2014) 611-623.
[39] T.H. Hui, Z.L. Zhou, J. Qian, Y. Lin, A.H. Ngan, H. Gao, Volumetric deformation of live cells induced by pressure-activated cross-membrane ion transport, Phys. Rev. Lett., 113 (11) (2014) 118101.
[40] Y. Yang, H. Jiang, Shape and Dynamics of Adhesive Cells: Mechanical Response of Open Systems, Phys. Rev. Lett., 118 (20) (2017) 208102.
[41] A.J. Engler, C. Caragkrieger, C.P. Johnson, M. Raab, H.Y. Tang, D.W. Speicher, J.W. Sanger, J.M. Sanger, D.E. Discher, Embryonic cardiomyocytes beat best on a matrix with heart-like elasticity: scar-like rigidity inhibits beating, J. Cell. Sci., 121 (22) (2008) 3794-3802.
[42] J. Solon, I. Levental, K. Sengupta, P.C. Georges, P.A. Janmey, Fibroblast Adaptation and Stiffness Matching to Soft Elastic Substrates, Biophys. J., 93 (12) (2007) 4453-4461.
[43] J.P. Marquez, G.M. Genin, K.M. Pryse, E.L. Elson, Cellular and Matrix Contributions to Tissue Construct Stiffness Increase with Cellular Concentration, Ann. Biomed. Eng., 35 (2) (2007) 320-320.
[44] J. Zhu, T. Li, S. Cai, Z. Suo, Snap-through Expansion of a Gas Bubble in an Elastomer, Journal of Adhesion, 87 (5) (2011) 466-481.
[45] D.L. Henann, K. Bertoldi, Modeling of elasto-capillary phenomena, Soft Matter, 10 (5) (2014)

709.
[46] S. Kundu, A. Crosby, Cavitation Rheology and Fracture Behavior of Polyacrylamide Hydrogels, Soft Matter, 5 (20) (2009) 3963-3968.
[47] A.L. Bug, S.A. Safran, G.S. Grest, I.I. Webman, Do interactions raise or lower a percolation threshold?, Phys.rev.lett, 55 (18) (1985) 1896.

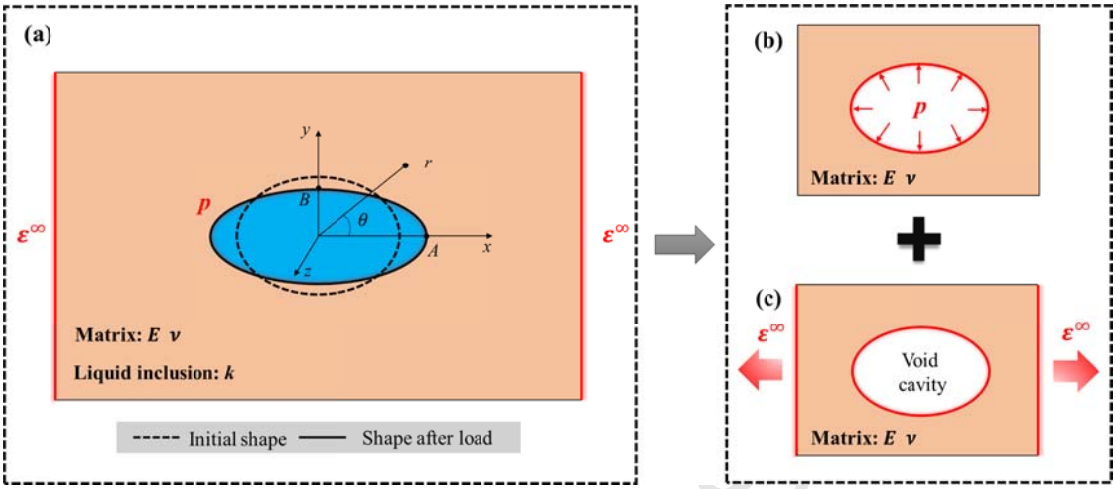

Figure 1. Schematic diagram of the problem. (a) An ellipsoidal, compressible liquid inclusion embedded within a linear-elastic solid subjected to a far field load. The solution can be treated as the superposition of solutions to two sub-problems: a void cavity subjected to an inner pressure (b) and a void cavity within a linear-elastic solid subjected to a far field load (c).

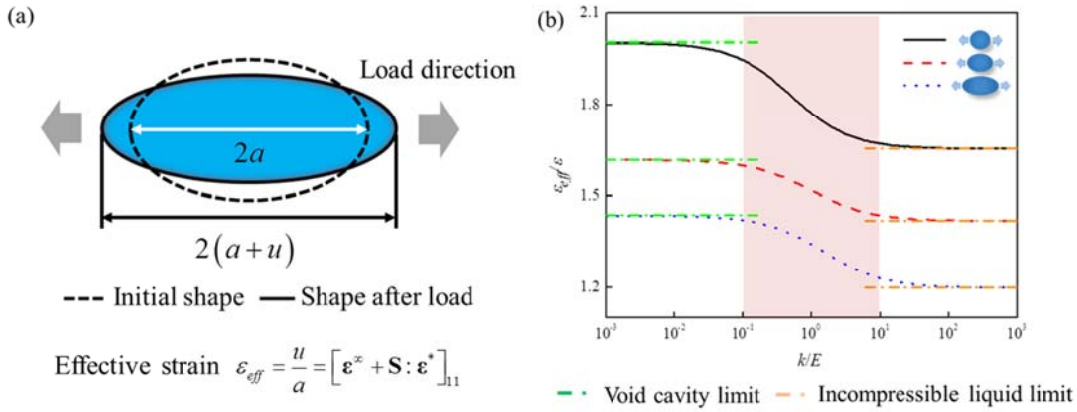

Figure 2. Deformation analysis of ellipsoidal liquid inclusions with different shape. (a) Effective strain is defined to characterize the sensitivity of the axial deformation of the inclusion to far field load in the load direction. (b) The compressibility affects the effective strain of ellipsoidal inclusions with different shape. The ratio of axial length is 1:1:1, 1.5:1:1 and 2:1:1, respectively. The load direction is along the longest axis. Shaded area represents the region where the value changes most. Green lines represent the cases of void cavity limit and orange lines represents the cases of incompressible limit. The data of limit cases are chosen from [9, 15, 24].

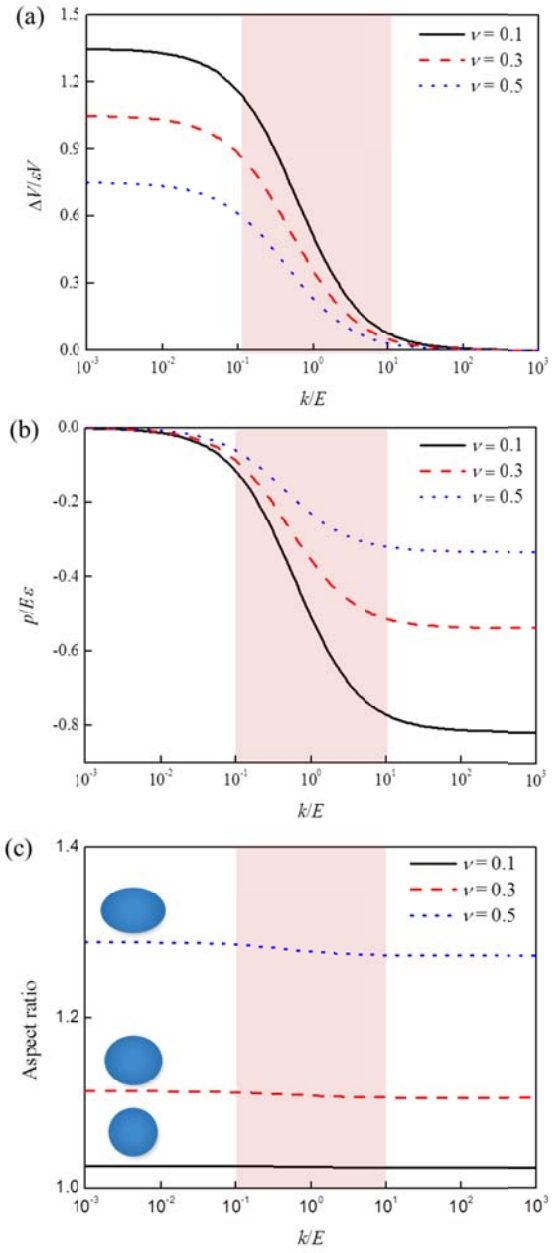

Figure 3. The effect of liquid compressibility on the mechanical behavior of a spherical inclusion. The normalized volume change of (a) and pressure within (b) a liquid inclusion are strong functions of the normalized compressibility of the inclusion. However, the post-loading aspect ratio (c) of the inclusion is not. Different lines represent different Poisson ratios of the matrix. The shaded area represents the region of highest sensitivity, which is the decade above and below that at which the moduli of the inclusion and matrix match.

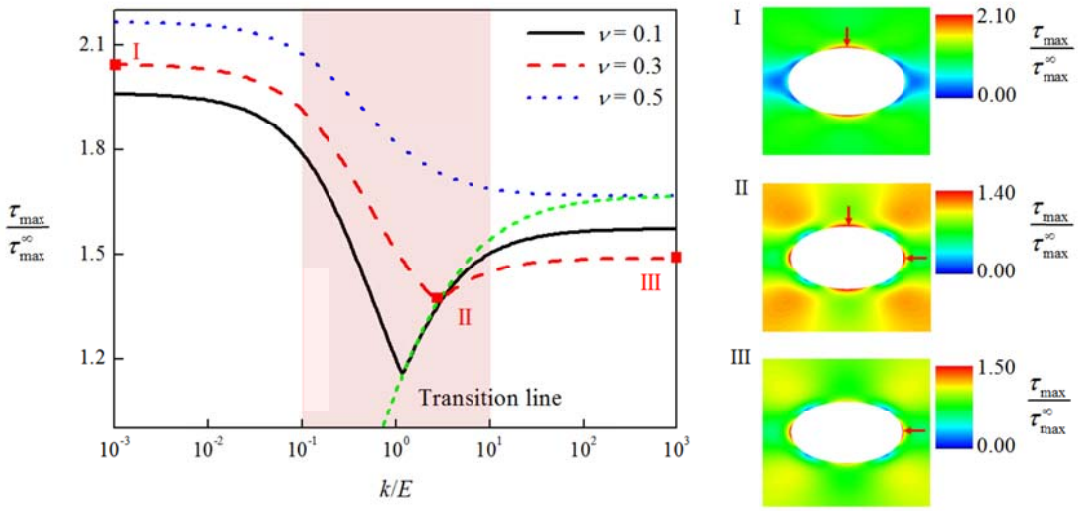

Figure 4. The maximum shear stress in the matrix is dependent on liquid compressibility. Different lines represent different Poisson ratios of the matrix. The shaded area represents the region of highest sensitivity. Panels I, II and III represent separately the normalized maximum shear stress $\tau_{\max}/\tau_{\max}^{\infty}$ near the inclusion with three different values of liquid compressibility. The location of the maximum shear stress (red arrows) changes from I to III as the liquid compressibility increases. Along the transition line, the maximum shear stress is minimized. This reduction in stress can enable strengthening of a composite material.

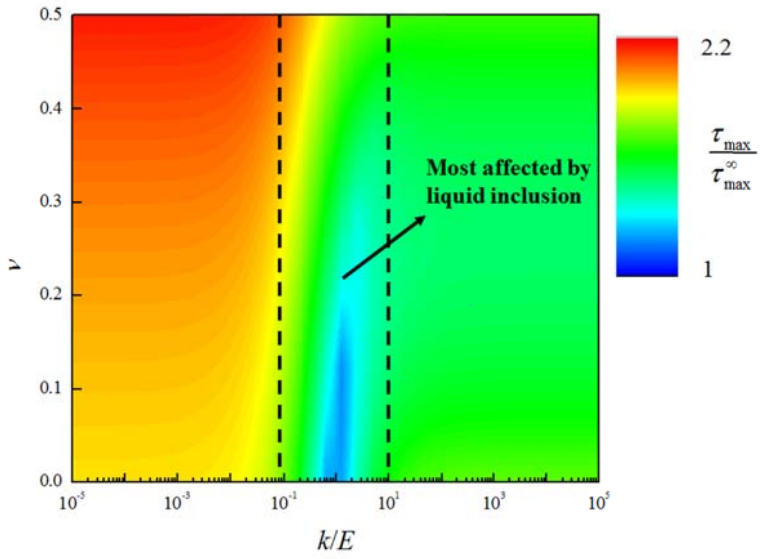

Figure 5. The maximum shear stress as a function of the ratio of liquid bulk modulus to the solid elastic modulus and Poisson ratio. In the region of sensitivity between the two dashed lines ($k/E \sim 1$), the maximum shear stress is sensitive to the ratio of the liquid bulk modulus to the solid elastic modulus. There is a minimum $\tau_{\max}/E\varepsilon$ as $k/E \sim 1$. This attenuation of stress increases substantially when the solid Poisson ratio is small (< 0.2).

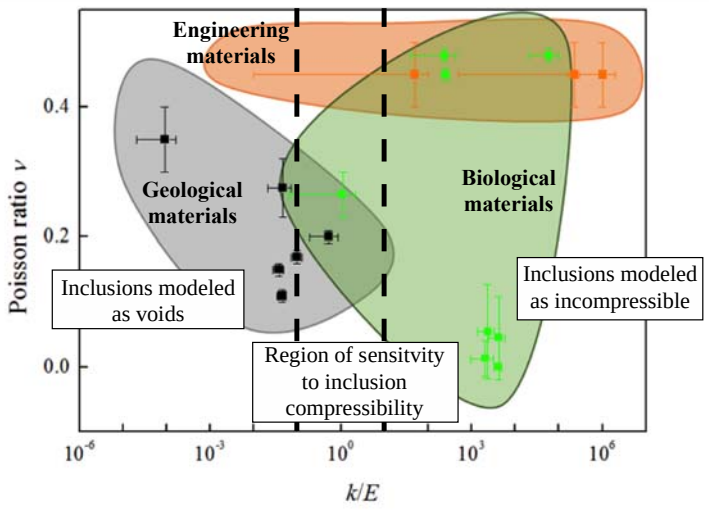

Figure 6. An Ashby-type representation of the ranges of liquid inclusions within a solid matrix for which compressibility plays an important role. These examples are classified into three board categories. *i.e.*, geological, biological and engineering materials. References are listed in the **Supplementary material**.